frontiers in Earth Science

ORIGINAL RESEARCH
published: 20 March 2020
doi: 10.3389/feart.2020.00078

Study on "Triaxial Loading-Unloading-Uniaxial Loading" and Microscopic Damage Test of Sandstone

Chao Yuan[1,2,3], Yuning Guo[3], Wenjun Wang[1,2,3], Liming Cao[3], Lei Fan[3] and Cong Huang[3]*

[1] Work Safety Key Lab on Prevention and Control of Gas and Roof Disasters for Southern Coal Mines, Xiangtan, China, [2] Hunan Key Laboratory of Safe Mining Techniques of Coal Mines, Xiangtan, China, [3] School of Resources, Environment and Safety Engineering, Hunan University of Science and Technology, Xiangtan, China

To study the weakening process, deformation, and failure characteristics of rock masses surrounding deep chambers under complex stress environments, triaxial loading tests along with triaxial loading/unloading followed by uniaxial loading tests were conducted on sandstone specimens. The internal microcracks of the specimens under the loading and unloading of triaxial confining pressure were observed by scanning electron microscopy. The results revealed the inherent mechanism of plastic deformation (irreversible deformation) of the rock mass under different confining pressures. Under uniaxial loading and triaxial loading, the sandstone specimens exhibited X-shaped shear failure and single shear failure, respectively. In contrast, the sandstone samples subjected to the loading and unloading of triaxial confining pressure followed by uniaxial loading showed multiple shear fracture surfaces and fine fissures along the axial direction. A larger initial axial pressure of the sandstone specimen corresponded to a smaller uniaxial loading strength after unloading the confining pressure, a greater amount of plastic deformation, more macro- and microfissures, and more severe damage to the specimen. These results show that the final failure mode, strength, degree of damage, and plastic deformation of sandstone specimens are related to the stress state at the time of failure along with the loading history before failure.

Keywords: strength, plastic deformation, failure pattern, macrofissure, microfissure

OPEN ACCESS

Edited by:
Lianyang Zhang,
University of Arizona, United States

Reviewed by:
Jie Liu,
Hunan Institute of Engineering, China
Yao Qi,
Hunan City University, China

****Correspondence:***
Chao Yuan
yuanchaozh1@126.com

Specialty section:
This article was submitted to Earth and Planetary Materials, a section of the journal Frontiers in Earth Science

Received: *10 January 2020*
Accepted: *05 March 2020*
Published: *20 March 2020*

Citation:
Yuan C, Guo Y, Wang W, Cao L, Fan L and Huang C (2020) Study on "Triaxial Loading-Unloading-Uniaxial Loading" and Microscopic Damage Test of Sandstone. Front. Earth Sci. 8:78. doi: 10.3389/feart.2020.00078

INTRODUCTION

The excavation of deep underground chambers changes the stress state of the surrounding rock and causes the peak stress value in the surrounding rock to shift toward greater depth. This process is usually accompanied by disturbances (e.g., rheological and seepage) and results in rock burst, spallation, plate fracture, and other forms of rock failure and instability. These effects have serious consequences for construction speed, quality, and safety (Yu et al., 2019; Yuan et al., 2020). The failure and instability of the rock surrounding deep chambers are essentially products of a gradual process in which the rock mass develops mesodamage and macrofractures under the action of secondary stress. The mechanics of this process are derived from the different degrees of stress unloading and reloading during the course of stress adjustment in a state of high three-dimensional stress. The mechanical properties of the

rock mass are closely related to its loading history and are fundamentally different from those of a rock mass under monotonic or constant load. Therefore, to accurately analyze the stability of the chamber-surrounding rock mass, it is necessary to study the macro and meso deformation failure characteristics along with the weakening processes of rock masses under various loading and unloading modes.

Numerous studies have evaluated the mechanical responses and damage characteristics of rock masses under loading and unloading, providing important reference data (Zhao et al., 2016, 2019b). Zhou et al. (2020) studied the internal stress distribution and failure characteristics of cylindrical cavities under triaxial cyclic loading and found that the number of cracks in the rock mass increased as the triaxial loading progressed, accompanied by plastic deformation. Yang et al. (2009) comparatively studied salt rock deformation characteristics under uniaxial loading along with cyclic loading and unloading. The authors found that the deformation parameters were more regular under cyclic unloading and reloading compared to under uniaxial stress–strain. Fuenkajorn and Phueakphum (2010) carried out uniaxial cyclic loading and unloading tests on salt rocks to study the effects of cyclic loading on the uniaxial compressive strength, elastic modulus, and irreversible deformation of rock masses. The results showed that the compressive strength of the rock mass decreased continuously with the number of cyclic loadings, and the elastic modulus was limited by the number of cyclic loadings. Zhou et al. (2014) studied the brittle failure characteristics and mechanical deformation mechanism of granite under different confining pressures through triaxial compression tests and scanning electron microscopy (SEM) analyses of fracture surfaces. Fan et al. (2019) used a combination of rock mechanics tests and numerical simulations to study how the degree of weathering affects the shear behavior and mechanical properties of rock masses. The authors also observed the initiation, propagation, and consolidation of cracks. Liu and Li (2018) simulated triaxial cyclic loading and unloading tests on marble using a particle flow program. They found that many cracks appeared in the marble during cyclic loading, and the number of cracks exhibited good "memory" behavior at the initial stage of loading. When the load entered the plastic zone, "non-memory" behavior gradually appeared. Gao et al. (2018) studied the mechanical properties, failure modes, and effects of confining pressure during the uniaxial and triaxial compression tests of marble specimens and obtained the brittle transition characteristics of marble with increasing confining pressure. Shen et al. (2019) prepared a single-joint sandstone specimen and found that the specimen exhibited irreversible plastic deformation during the early stage of cyclic loading and unloading. Fan et al. (2018) carried out loading and unloading tests on cubic red sandstone specimens and analyzed their strength characteristics under loading and unloading conditions; they found that the unloading effect was related to the end-point stress state along with the stress state and unloading path before failure. Li et al. (2018) carried out triaxial compression tests along with cyclic loading and unloading tests on frozen saturated sandstone specimens and analyzed the strength characteristics of the specimens under different confining pressures. They found that the peak intensity of the rock mass under low confining pressure increased during cyclic loading and unloading, and the peak intensity appeared to weaken under high confining pressure. Du et al. (2016) studied the effect of intermediate principal stress on the rupture of the fracture plate of the rock mass through triaxial compression tests. Gong et al. (2019) conducted a triaxial compression test on a rock mass to study the effect of intermediate principal stress on plate fracture. Under the initial stress conditions

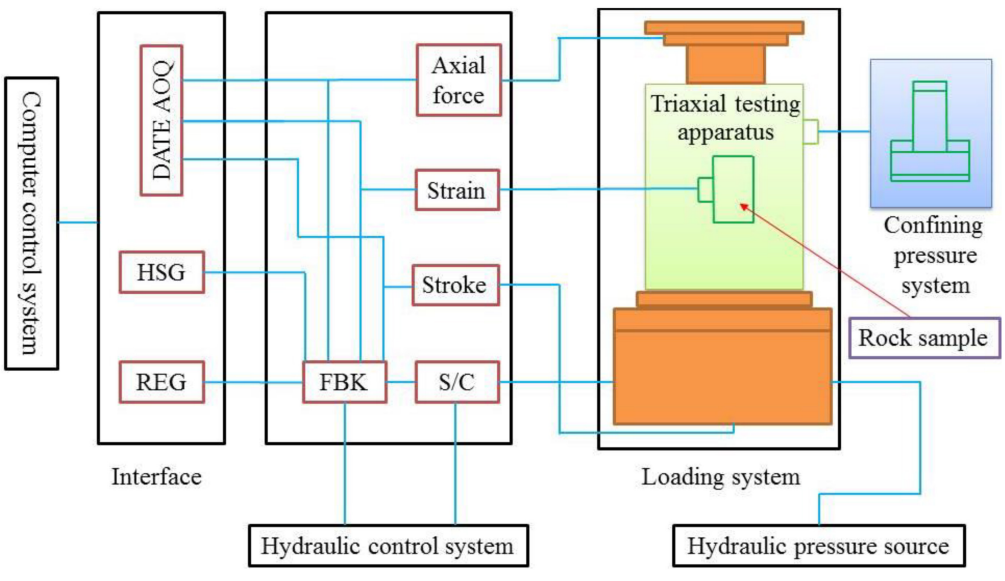

FIGURE 1 | Schematic of the deformation test system.

of triaxial loading, the intermediate principal stress remained unchanged, the minimum principal stress was rapidly unloaded, and the maximum principal stress slowly increased. The failure mode of the rock mass was found to be shear failure when the intermediate principal stress was small, whereas the failure mode was plate fracture when the intermediate principal stress was large. Zhao et al. (2019a) conducted Brazilian split tests on sandstone specimens treated with hot water to study the relationship between stress/strain and temperature. They also used SEM to observe the sandstone specimens treated at high temperature and high pressure. Wu et al. (2019) conducted Brazilian split tests on granite specimens after heating and cooling treatments and analyzed the effects of these treatments on the P-wave velocity, microcracks, tensile strength, and fracture roughness of the samples. Amitrano and Schmittbuhl (2002) employed SEM to analyze the microcharacteristics of the rock shear fracture zone resulting from crack initiation, propagation, nucleation, and microcrack penetration. Based on triaxial loading and unloading tests on marble and granite, Li et al. (2016) investigated the evolution of rock energy in the unloaded state along with the mechanical characteristics of rock failure under different pathways. Through various loading and unloading tests under different rates, stresses, and stress differences, Zhang et al. (2012) obtained the deformation, failure, and strength characteristics of soft and hard rocks represented by siltstone and granite, respectively, under complicated conditions. Wang et al. (2019) found that soft rock undergoes shear failure under loading and unloading conditions, with essentially no microcrack formation with the exception of the main cracks during loading. When unloading, secondary cracks were more developed after rock sample failure at low unloading stress rates. Zuo et al. (2013) studied the rock deformation characteristics and pattern of strength change under different unloading rates. Deng et al. (2019) found that the failure modes of intermittent joint sandstones can be divided into three types: tensile failure, polyline-type composite shear failure, and shear failure along the joint plane. Zheng et al. (2019) studied the spatiotemporal changes in the water contents of coal samples before and after water immersion along with the characteristics of crack propagation and failure. They found that increasing the water content promoted a transition in the macroscopic failure mode from tensile failure to tensile shear composite failure. Using on-site-collected shale and limestone samples that were "spliced" into six different combinations of layered composite rock masses via indoor processing, Teng et al. (2018) analyzed the development of internal cracks before and after specimen rupture. Wang et al. (2018) studied the effects of joint interactions on the mechanical behavior of rock masses. They found that joint specimens could be divided into four failure modes under compression and shear loading: coplanar shear failure, shear failure along joint surfaces, shear failure along shear–stress surfaces, and intact shear failure. Through laboratory-based rock mechanics experiments, Zhao et al. (2017, 2019c) found that the instantaneous deformation and creep deformation of the rock mass are closely related to the deviatoric stress. High deviatoric stress is the main reason for the instability of the rock surrounding the deep chamber. Ding et al. (2019) studied the internal mechanism of irreversible deformation in rock specimens during the loading and unloading of confining pressure from a microscopic perspective. The irreversible deformation caused by skeleton particle displacement and the increase in rock compactness were found to cause the irreversible permeability.

In summary, previous studies mainly focused on the characteristic responses of rock stress, strain, and energy during the unloading processes of rock masses. However, few studies have been reported on the entire process of unloading after confining pressure of that. Toward this end, we carried out triaxial loading tests along with triaxial confining pressure loading/unloading tests followed by uniaxial loading using sandstone specimens. Furthermore, SEM was used to observe the microcracks in sandstone specimens under the loading and unloading of triaxial confining pressure. The deformation and failure, strength, and internal damage characteristics of rock masses under different stress pathways were then analyzed. The results provide guidance for the prevention and control of disasters related to the rock surrounding deep underground chambers.

MATERIALS AND METHODS

Principle of Sandstone Loading and Unloading Tests

The deformation of the rock surrounding deep underground chambers is primarily caused by the plastic deformation, expansion deformation, and bulge deformation of the rock mass in the crushed area and the plastic area. The rock mass in the fragmentation zone on the surface of the chamber rock is in a

TABLE 1 | Conditions of triaxial loading/unloading tests and uniaxial loading tests under different confining pressures.

Experimental program	Axial pressure	Confining pressure	Loading and unloading rate
Conventional triaxial loading test	–	0 MPa	
	–	5 MPa	
	–	10 MPa	0.05 MPa/s
	–	15 MPa	↓
	–	20 MPa	0.1 kN/s
	–	25 MPa	↓
	–	30 MPa	0.001 mm/s
	–	35 MPa	
	–	40 MPa	
Constant axis unloading confining pressure test	20 kN	30 MPa	0.1 kN/s
	30 kN		↓
	40 kN		0.005 MPa/s
↓	50 kN		↓
			0.01 kN/s
Uniaxial loading test	–	0 MPa	0.2 kN/s
	–		
	–		
	–		

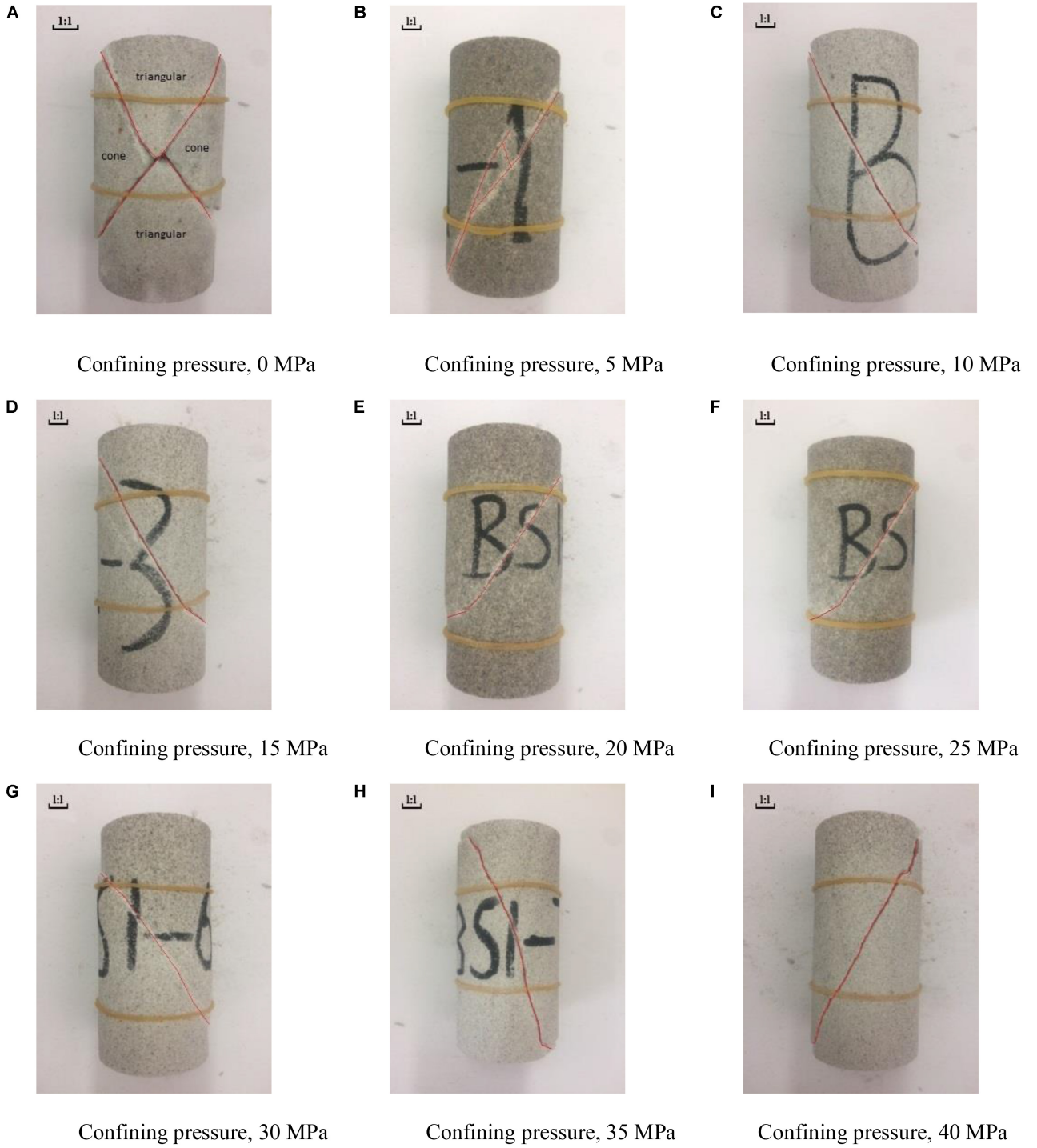

FIGURE 2 | Sandstone failure morphologies under uniaxial and triaxial loading. **(A)** Confining pressure, 0 MPa; **(B)** Confining pressure, 5 MPa; **(C)** Confining pressure, 10 MPa; **(D)** Confining pressure, 15 MPa; **(E)** Confining pressure, 20 MPa; **(F)** Confining pressure, 25 MPa; **(G)** Confining pressure, 30 MPa; **(H)** Confining pressure, 35 MPa; **(I)** Confining pressure, 40 MPa.

state of low confining pressure or even a state of uniaxial loading (the rock mass in the complete area with regional breakdown can also be approximated as a state of uniaxial loading). The radial stress in the chamber is the minimum principal stress, while the hoop stress is the maximum principal stress. Under different confining pressures, the stress environment of the rock mass in the plastic zone is triaxial loading. During the mining of a coal face, the unidirectional or triaxial stress reloading

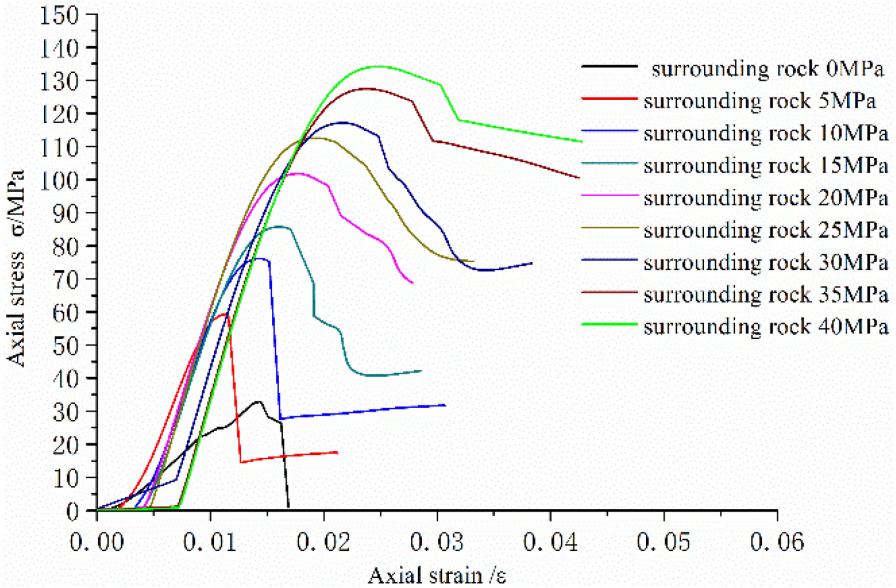

FIGURE 3 | Stress–strain curves of sandstone specimens under different confining pressures.

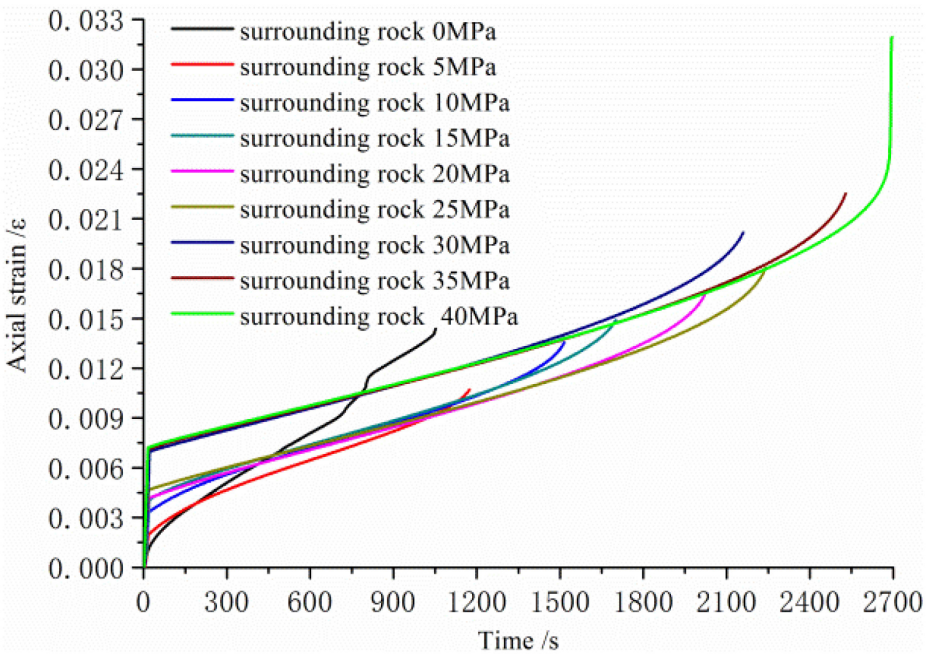

FIGURE 4 | Curves of axial strain vs. time for sandstone specimens under different confining pressures.

of the rock mass in the crushed area and the plastic area of the chamber rock is transferred by advance support pressure transfer. According to the stress changes during the excavation of the rock surrounding the deep chamber and the mining of the coal face, the process of mechanical deformation can be divided into three stages: (1) the high-stress triaxial loading stage, which corresponds to the loading history before the excavation of deep rock masses; (2) the unloading stage, which corresponds to the stress caused by chamber excavation; and (3) the reloading stage, which corresponds to the increase in advanced support pressure during the mining of the face. Therefore, it is necessary to subject samples to the loading and unloading of triaxial confining pressure followed by uniaxial loading and reproduce the stress state along with the deformation and failure characteristics of the rock surrounding the deep underground chamber.

Experimental Design for Sandstone Loading and Unloading Tests

The experimental rock mass was white sandstone with high homogeneity, few natural joints, and good integrity. Testing was carried out using a MTS815 rock mechanics test system with four independent control systems: axial pressure, confining pressure, pore water pressure, and temperature. The overall stiffness of the testing machine frame was 10.5 × 109 N/m, and its maximum axial force was 4600 kN. The maximum confining pressure was 140 MPa, and the long-term stability of the axial and confining pressures was ≤± 1%. The axial and radial strains of the rock specimen during deformation were measured using a built-in axial extensometer and chain hoop extensometer. **Figure 1** shows a schematic diagram of the deformation test system. The testing process consisted of the following steps.

(1) A set of standard test specimens was selected for triaxial loading under different confining pressures of 0, 5, 10, 15, 20, 25, 30, 35, and 40 MPa. The test piece was first loaded with an axial pressure of 1.5 kN, and the axial and confining pressures were then loaded at a rate of 0.05 MPa/s. After the confining pressure was loaded to the preset value, an axial pressure was applied at a rate of 0.1 kN/s, and the load was brought close to the peak intensity of the test piece. When the axial stress was loaded to 98% of the peak strength, the displacement loading control method was applied, and the loading rate was maintained at 0.001 mm/s until the rock specimen was destroyed. For each test, the average value of three specimens was taken as the peak stress.

(2) According to the peak intensity obtained in step (1), taking into account the ground stress conditions of underground engineering, and based on the peak sandstone intensity at a confining pressure of 30 MPa, axial pressure was applied at a rate of 0.1 kN/s. The test specimens were loaded with predetermined pressures of 20, 30, 40, and 50 kN (i.e., the stress state before sample failure) (Liu et al., 2017), and the confining pressure was unloaded directly after stabilization for 10 min at an unloading rate of 0.005 MPa/s. Subsequently, the axial pressure was unloaded at an unloading rate of 0.01 kN/s.

(3) The sandstone specimens that were not damaged in step (2) were subjected to uniaxial loading tests. The specimens were loaded until failure by applying axial pressure at a rate of 0.2 kN/s.

Table 1 shows the initial stress levels, loading and unloading types, and loading and unloading rates used in the deformation tests.

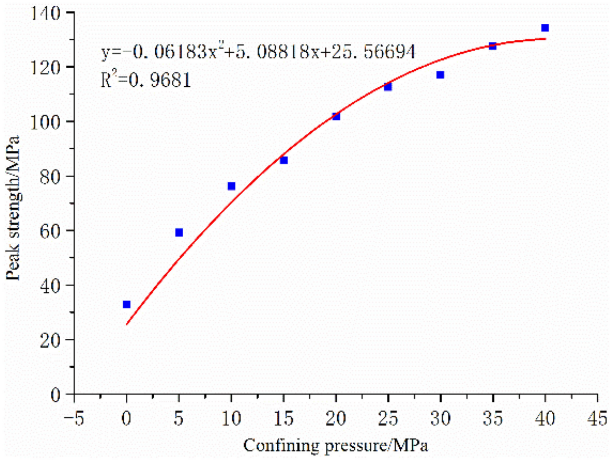

FIGURE 5 | Curve of peak strength vs. confining pressure.

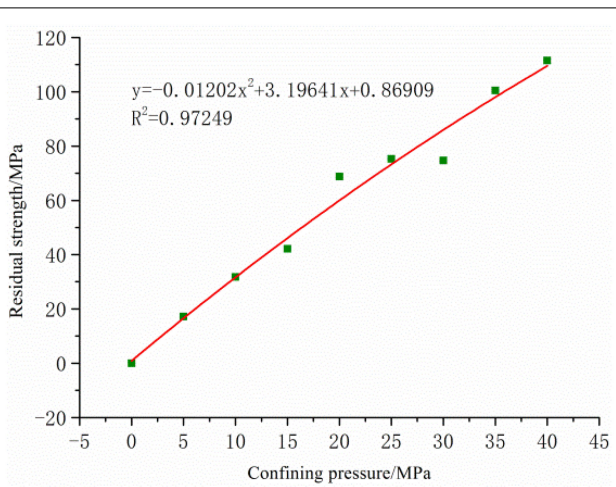

FIGURE 6 | Curve of residual strength vs. confining pressure.

RESULTS

Uniaxial and Triaxial Loading Tests

Sandstone Failure Morphology

After failure under uniaxial loading, the sandstone specimens were block shaped and could mostly be divided into four blocks: two "cone" blocks at the upper and lower ends of the test piece and two "triangular" blocks at the left and right ends of the test piece. As a whole, the specimens exhibited X-shaped shear failure, as shown in **Figure 2A**. Compared with the test piece subjected to uniaxial loading, the specimens under different confining pressures showed obvious single-shear slip failure, with the fracture surface sheared along a single bevel and the test piece divided into two triangular pyramid-shaped fractured blocks; thus, the failure mode was shear failure, as shown in **Figures 2B–I**.

Stress and Strain Characteristics of Sandstone

The stress–strain curves of sandstone samples under different confining pressures are shown in **Figure 3**. The steepness of the stress–strain curve increased with increasing confining pressure, corresponding to increased elastic modulus and greater resistance of the rock body to deformation and failure. Under low confining pressure, the sandstone exhibited obvious brittle

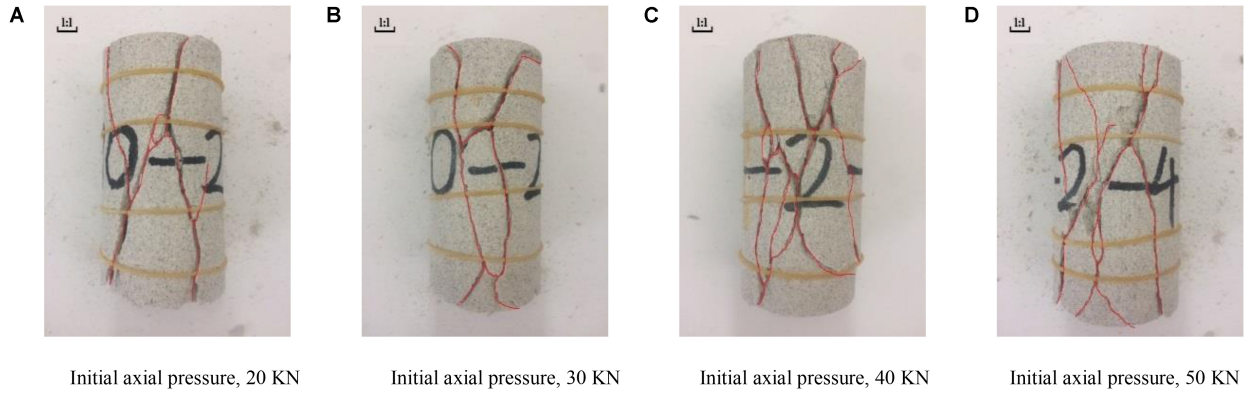

FIGURE 7 | Failure patterns of white sandstone samples subjected to the loading and unloading of triaxial confining pressure followed by uniaxial compression. **(A)** Initial axial pressure, 20 kN; **(B)** Initial axial pressure, 30 kN; **(C)** Initial axial pressure, 40 kN; **(D)** Initial axial pressure, 50 kN.

failure characteristics after the peak in the stress–strain curve. For example, when the confining pressure was 5 MPa, the failure mode of the rock mass was brittle failure, and a rather large decrease in stress was observed. As the confining pressure gradually increased, ductile failure characteristics began to appear after the peak in the curve, and the ductile characteristics became more obvious with increasing confining pressure. For example, when the confining pressure was increased to 25 MPa, the deformation and failure of sandstone showed obvious ductile characteristics, and the large-scale decrease in stress disappeared.

The curves of axial strain vs. time are shown in **Figure 4** for different confining pressures. Under the same loading rate, the axial strain of the sandstone specimen increased with increasing confining pressure, and the change in axial strain could be divided into the following three stages. (1) In the deceleration and deformation phase, axial strain decreased with increasing axial stress (i.e., convex relationship); however, due to the effects of test prestress and hydrostatic pressure, this phase gradually disappeared as the confining pressure increased. (2) In the stable deformation stage, the stress–strain curve of the rock mass was approximately linear; this stage was extended as the confining pressure increased. (3) During the accelerated deformation phase, the axial stress continued to increase, and the axial strain increased rapidly along the axial direction of the specimen, causing the sandstone to quickly fracture and become unstable.

MATLAB software was used to describe the relationships between peak strength and confining pressure and between residual strength and confining pressure (**Figures 5**, **6**). The peak and residual strengths of the sandstone specimens increased parabolically with increasing confining pressure. A higher confining pressure corresponded to higher peak and residual strengths of specimen failure; however, the peak intensity gradually decreased with the rate of increase in confining pressure.

For an underground chamber, if the support resistance is regarded as the confining pressure, increasing the support resistance will increase the peak strength of the surrounding rock. To some extent, increasing the support resistance is helpful for increasing the peak strength and residual strength of the surrounding rock and for enhancing the ability of the surrounding rock to resist damage.

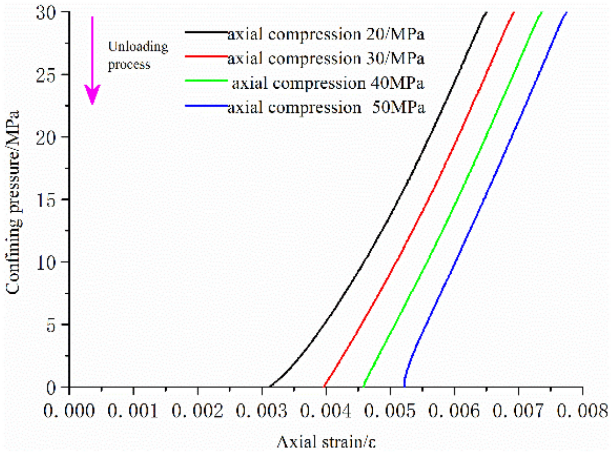

FIGURE 8 | Curves of confining pressure during the unloading process vs. axial strain for different initial axial pressures.

Triaxial Loading/Unloading Followed by Uniaxial Loading

Sandstone Failure Morphology

The average peak strength of the sandstone specimen under a confining pressure of 30 MPa was 117.1 MPa. Based on this peak strength, the specimens were subjected to the loading and unloading of triaxial confining pressure followed by uniaxial loading with different values of initial axial compression.

As shown in **Figure 7**, unlike the sandstone specimens under uniaxial loading and triaxial loading under multiple confining pressures (see **Figure 2**), the failure morphology of the rock mass subjected to the loading/unloading of triaxial confining pressure followed by uniaxial compression was clearly different. In addition to the main shear failure surface, two or more fissures ran through the entire specimen. A small number of local shear

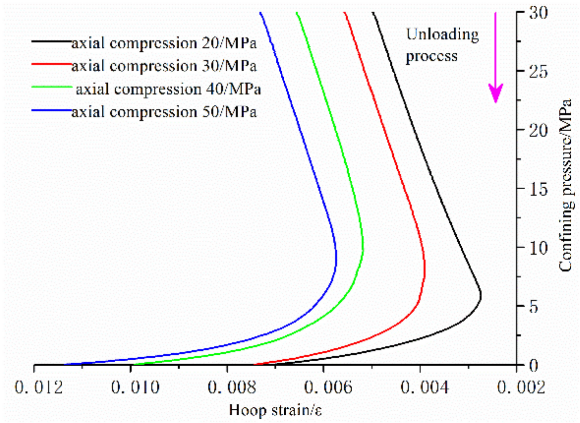

FIGURE 9 | Curves of confining pressure during the unloading process vs. hoop strain for different initial axial pressures.

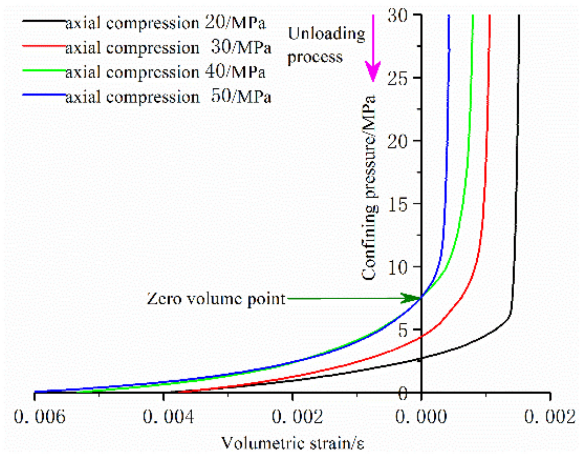

FIGURE 10 | Curves of confining pressure during the unloading process vs. volumetric strain for different initial axial pressures.

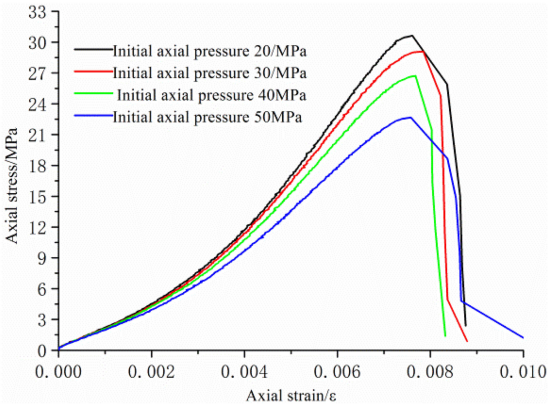

FIGURE 11 | Uniaxial compressive stress–strain curves.

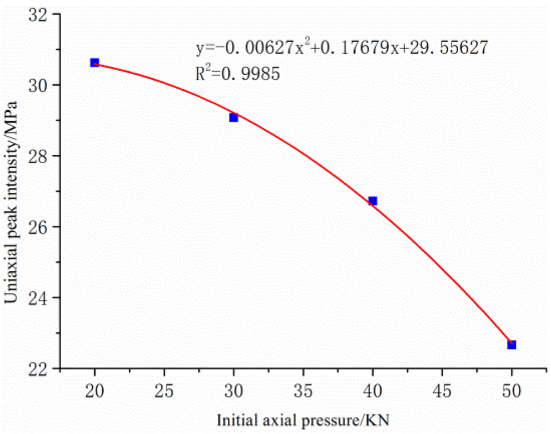

FIGURE 12 | Relationship between uniaxial peak intensity and initial axial pressure.

failure surfaces were observed, and fine cracks appeared along the direction of axial stress in the specimen. The cracks intersected each other, and the number of cracks increased with increasing initial axial pressure.

Based on failure surface and the number of macrocracks, the failure mode of the rock mass was not only related to the stress state at the time of final failure; it was also strongly related to the loading and unloading history and corresponding stress level of the rock mass. The history of loading and unloading will inevitably cause some damage to the rock mass.

Stress and Strain Characteristics of Sandstone Under Confining Pressure

Figure 8 shows the relationship between the confining pressure during the unloading process and the axial strain for sandstone samples with different initial axial compression. Due to the different initial values of axial compressive stress, the axial strains at the initial stage of confining pressure unloading differed. Thus, the axial strain of the initial stage of confining pressure unloading increased with increasing initial axial pressure. The axial strain of the rock mass decreased in an approximately linear fashion as the confining pressure was unloaded. When the confining pressure of the rock mass was unloaded to 0 MPa, the axial strain was not reduced to zero. This indicates that under the action of confining pressure, axial deformation can be divided into two parts: recoverable elastic deformation and unrecoverable plastic deformation. Plastic deformation increased with increasing initial axial pressure.

Figure 9 shows the curves of confining pressure during the unloading process vs. hoop strain for different initial axial pressures. Similar to the curves shown in **Figure 8**, the hoop strain corresponding to the initial confining pressure increased with the initial axial pressure and decreased linearly as the confining pressure was unloaded. This indicates the presence of some recoverable elastic deformation in the hoop direction. When the unloading confining pressure reached a certain critical value, the hoop strain curve shifted toward the left, and hoop strain began to increase linearly. When the confining pressure

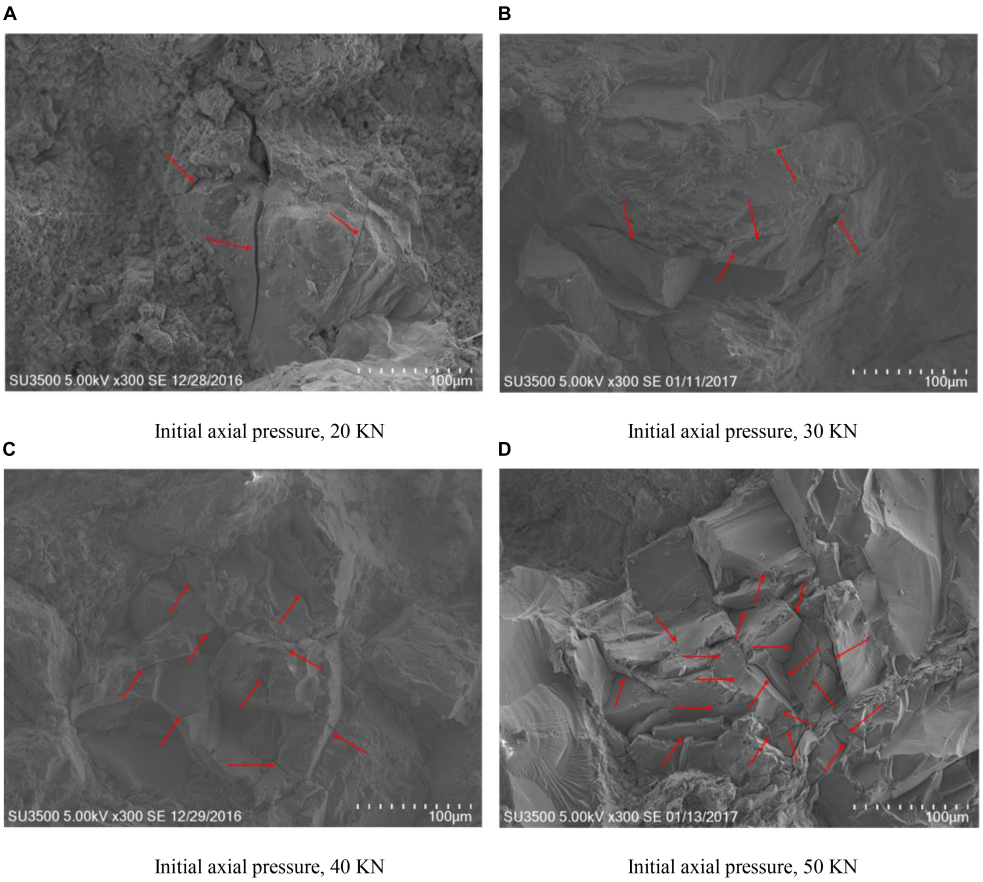

FIGURE 13 | SEM images showing the internal damage of the rock mass under different initial axial compression levels. **(A)** Initial axial pressure, 20 kN; **(B)** Initial axial pressure, 30 kN; **(C)** Initial axial pressure, 40 kN; **(D)** Initial axial pressure, 50 kN.

was unloaded to 0 MPa, the hoop strain increased with increasing initial axial pressure. Compared to the hoop strain of the rock mass during the initial and final unloading of confining pressure, although no significant damage occurred, the unloading caused some unrecoverable deformation in the hoop of the rock mass (i.e., plastic deformation).

Figure 10 shows the curves of confining pressure during the unloading process vs. volumetric strain. In the initial stage of confining pressure unloading, the volumetric strain remained essentially unchanged. When the confining pressure was unloaded to a certain value, the volumetric strain began to decrease rapidly to the zero-volume point and then increased continuously as confining pressure continued to be unloaded; a significant capacity expansion phenomenon was observed.

Stress and Strain Characteristics of Sandstone Under Uniaxial Loading

Figure 11 shows the stress–strain curves of uniaxial loading after the confining pressure of sandstone specimens was unloaded under different initial axial pressures. As shown in **Figure 12**, when the confining pressure was 30 MPa, a higher initial axial load corresponded to a lower sandstone specimen strength after the unloading of confining pressure followed by uniaxial loading. Furthermore, the peak intensity decreased in a non-linear fashion as the initial axial pressure increased.

According to the above results, the loading history of sandstone affects the strength of the rock mass along with the degrees of damage and plastic deformation. The number of macroscopic fractures in the rock mass increased with increasing initial axial pressure. For deep, high-stress chambers, although the rock mass around the excavated chamber may not experience macrodamage, mining and other influences often cause a certain degree of damage to the interior of the rock mass, and the strength of the rock mass is weakened to a large extent upon the unloading of the confining pressure. This is one of the main reasons for the difficulty in predicting and effectively controlling disasters in the rock masses surrounding high-stress chambers.

Analysis of Mesodamage Based on the Results of Sandstone Loading and Unloading Tests

Sandstone Mesocracking Observation Equipment

Based on the above analysis, the uniaxial compressive strength of the sandstone specimen gradually decreased with increasing initial axial pressure, indicating that different initial axial

pressures cause different degrees of damage to the rock mass. To reveal the mesodamage mechanism of sandstone under different initial axial compression levels, another white sandstone specimen was subjected to a triaxial confining pressure loading–unloading test. The unloaded test piece was cut with a small cutting machine, and the cutting surface was observed by SEM using a SU3500 scanning electron microscope.

Microscopic Analysis of Sandstone Damage

Figure 13 shows SEM images depicting the internal damage to sandstone samples under different initial axial compressive stress levels. The red arrows refer to microfissures. When the initial axial pressure was 20 kN (**Figure 13A**), the rock surface exhibited two obvious microcracks. When the initial axial pressure was increased to 30 kN, the number of microfissures on the surface of the rock mass reached four (**Figure 13B**). When the initial axial pressure was increased to 40 or 50 kN, the number of microfissures on the surface of the rock mass exceeded 10 (**Figures 13C,D**). Thus, the number of microfractures on the surface of the rock mass increased gradually with increasing initial axial pressure. When the number of microfractures reached a certain value, interpenetration occurred between the microcracks, and the distribution was uneven.

The above results suggest that the loading/unloading history the rock masses surrounding deep underground chambers should not be ignored in efforts to prevent and control disasters in the surrounding rock. Even if the chamber rock does not exhibit macrocracks or damage, a certain amount of damage will be present inside the rock mass, and the number of microfractures that appear in the rock mass is closely related to the magnitude of the load.

CONCLUSION

(1) The sandstone specimens under uniaxial loading and triaxial loading showed X-shaped shear failure and single-shear failure modes. However, the samples subjected to the loading and unloading of triaxial confining pressure followed by uniaxial loading exhibited multiple fracture surfaces and fine secondary cracks along the axial direction of the specimen. The number of cracks gradually increased with increasing initial axial pressure.

(2) The peak strength of the sandstone specimen subjected to the loading and unloading of triaxial confining pressure followed by uniaxial loading increased with increasing initial axial pressure; however, the sensitivity of the increase decreased.

(3) The axial and circumferential deformation of sandstone specimens during the unloading of confining pressure could be divided into two parts: recoverable elastic deformation and non-recoverable plastic deformation. Plastic deformation increased with increasing initial axial pressure.

(4) Although the sandstone specimen did not exhibit macrocracks or damage after the process of triaxial compression loading/unloading, a certain degree of damage occurred inside the specimen, and microfissures were observed. The number of microfissures gradually increased as the initial axial pressure of the rock mass increased. The internal microstructural changes observed in the sandstone specimens were in good agreement with their plastic deformation.

DATA AVAILABILITY STATEMENT

All datasets generated for this study are included in the article/supplementary material.

AUTHOR CONTRIBUTIONS

CY and WW conceived and designed the experiments and contributed to funding supports. LC and CH performed the experiments. CY and LF analyzed the data. CY wrote the manuscript. YG revised the English language of the manuscript.

FUNDING

This work was financially supported by the National Natural Science Foundation of China (Grant Nos. 51804109, 51434006, and 51874130), the Scientific Research Fund of Hunan Provincial Education Department (Grant No. 18C0333), the Scientific Research Foundation for Doctor of Hunan University of Science and Technology (Grant No. E51851), and the Graduate Research and Innovation Project of Hunan (Grant No. CX20190794). The authors are grateful for this financial support.

REFERENCES

Amitrano, D., and Schmittbuhl, J. (2002). Fracture roughness and gouge distribution of a granite shear band. *J. Geophys. Res.* 107:2375. doi: 10.1029/2002JB001761

Deng, H., Pan, D., Xu, X., Zhi, Y., Duan, L., Yang, C., et al. (2019). Mechanical characteristics of intermittent jointed sandstone under triaxial compression. *Chin. J. Geotech. Eng.* 41, 2133–2141. doi: 10.11779/CJGE201911020

Ding, C., Zhang, Y., Yang, X., Hu, D., Zhou, H., and Lu, J. (2019). Permeability evolution of tight sandstone under high confining pressure and high pore pressure and its microscopic mechanism. *Rock Soil Mech.* 49, 3300–3308. doi: 10.16285/j.rsm.2018.1029

Du, K., Tao, M., Li, X., and Zhou, J. (2016). Experimental study of slabbing and rock burst induced by true-triaxial unloading and local dynamic disturbance. *Rock Mech. Rock Eng.* 49, 3437–3453. doi: 10.1007/s00603-016-0990-4

Fan, H., Sun, S., Le, H., Zhu, F., Wang, W., Liu, Y., et al. (2019). An experimental and numerical study of diorite-porphyrites with different weathered degree in the direct shear test. *Front. Earth Sci.* 7:352. doi: 10.3389/feart.2019.00352

Fan, P., Li, Y., Zhao, Y., Wang, M., Wang, D., and Shi, Y. (2018). Experimental study on unloading failure strength of red sandstone. *Chin. J. Rock Mech. Eng.* 37, 852–861. doi: 10.13722/j.cnki.jrme.2017.1368

Fuenkajorn, K., and Phueakphum, D. (2010). Effects of cyclic loading on mechanical properties of Maha Sarakham salt. *Eng. Geol.* 112, 43–52. doi: 10.1016/j.enggeo.2010.01.002

Gao, Y., Zhou, H., Zhang, C., Chen, J., He, S., and Liu, N. (2018). Research on the time-dependent strength criterion of brittle hard rock. *Chin. J. Rock Mech. Eng.* 37, 671–678. doi: 10.13722/j.cnki.jrme.2017.1075

Gong, F., Luo, Y., and Liu, D. (2019). Simulation tests on spalling failure in deep straight-wall-top-arch tunnels. *Chin. J. Geotech. Eng.* 41, 1091–1100. doi: 10.11779/CJGE201906013

Li, D., Sun, Z., Li, X., and Xie, T. (2016). Mechanical response and failure characteristics of granite under different stress paths in triaxial loading and unloading conditions. *Chin. J. Rock Mech. Eng.* 35(Suppl. 2), 3449–3457. doi: 10.13722/j.cnki.jrme.2016.0815

Li, T., Ma, Y., Liu, B., Sheng, H., and He, P. (2018). Strength characteristics and elastic modulus evolution of frozen gray sandstone under cyclic loading. *J. China Coal Soc.* 43, 2438–2443.

Liu, J., and Li, J. (2018). Analysis on meso-damage characteristics of marble under triaxial cyclic loading and unloading based on particle flow simulation. *J. Cent. South Univ. (Sci. Technol.)* 49, 2798–2803. doi: 10.11817/j.issn.1672-7207.2018.11.021

Liu, X., Liu, J., Li, D., He, C., Wang, Z., and Xie, Y. (2017). Experimental research on the effect of different initial unloading levels on mechanical properties of deep-buried sandstone. *Rock Soil Mech.* 38, 3081–3088. doi: 10.16285/j.rsm.2017.11.001

Shen, Y., Yang, H., Jin, L., Zhang, H., Yang, G., and Zhang, J. (2019). Fatigue deformation and energy change of single-joint sandstone after freeze-thaw cycles and cyclic loadings. *Front. Earth Sci.* 7:333. doi: 10.3389/feart.2019.00333

Teng, J., Tang, J., Wang, J., and Zhang, Y. (2018). The evolution law of the damage of bedded composite rock and its fractal characteristics. *Chin. J. Rock Mech. Eng.* 37 (Suppl. 1), 3263–3278. doi: 10.13722/j.cnki.jrme.2016.1397

Wang, F., Cao, P., Cao, R., Gao, Q., Xiong, X., and Wang, Z. (2018). Influence of parallel joint interaction on mechanical behavior of jointed rock mass. *J. Cent. South Univ. (Sci. Technol.)* 49, 2498–2507.

Wang, L., Niu, C., Zhang, B., Ma, Y., Yin, S., and Xu, X. (2019). Experimental study on mechanical properties of deep-buried soft rock under different stress paths. *Chin. J. Rock Mech. Eng.* 38, 973–981. doi: 10.13722/j.cnki.jrme.2018.0973

Wu, Q., Weng, L., Zhao, Y., Guo, B., and Luo, T. (2019). On the tensile mechanical characteristics of fine-grained granite after heating/cooling treatments with different cooling rates. *Eng. Geol.* 253, 94–110. doi: 10.1016/j.enggeo.2019.03.014

Yang, C., Ma, H., and Liu, J. (2009). Study of deformation of rock salt under cycling loading and unloading. *Rock Soil Mech.* 30, 3562–3568. doi: 10.16285/j.rsm.2009.12.027

Yu, W., Pan, B., Zhang, F., Yao, S., and Liu, F. (2019). Deformation characteristics and determination of optimum supporting time of alteration rock mass in deep mine. *KSCE J. Civ. Eng.* 23, 4921–4932. doi: 10.1007/s12205-019-0365-y

Yuan, C., Fan, L., Cui, J., and Wang, W. (2020). Numerical simulation of the supporting effect of anchor rods on layered and nonlayered roof rocks. *Adv. Civ. Eng.* 2020:4841658. doi: 10.1155/2020/4841658

Zhang, L., Wang, Z., Shi, L., and Kong, L. (2012). Acoustic emission characteristics of marble during failure process under different stress paths. *Chin. J. Rock Mech. Eng.* 31, 1230–1236. doi: 10.3969/j.issn.1000-6915.2012.06.019

Zhao, Y., Bi, J., Zhou, X., and Huang, Y. (2019a). Effect of high temperature and high pressure of water on micro-characteristic and splitting tensile strength of gritstone. *Front. Earth Sci.* 7:301. doi: 10.3389/feart.2019.00301

Zhao, Y., Wang, Y., and Tang, L. (2019b). The compressive-shear fracture strength of rock containing water based on druker – prager failure criterion. *Arab. J. Geosci.* 12:452. doi: 10.1007/s12517-019-4628-1

Zhao, Y., Wang, Y., Wang, W., Tang, L., Liu, Q., and Cheng, G. (2019c). Modeling of rheological fracture behavior of rock cracks subjected to hydraulic pressure and far field stresses. *Theor. Appl. Fract. Mech.* 101, 59–66. doi: 10.1016/j.tafmec.2019.01.026

Zhao, Y., Zhang, L., Wang, W., Pu, C., Wan, W., and Tang, J. (2016). Cracking and stress–strain behavior of rock-like material containing two flaws under uniaxial compression. *Rock Mech. Rock Eng.* 49, 2665–2687. doi: 10.1007/s00603-016-0932-1

Zhao, Y., Zhang, L., Wang, W., Tang, J., Lin, H., and Wan, W. (2017). Transient pulse test and morphological analysis of single rock fractures. *Int. J. Rock Mech. Min. Sci.* 91, 139–154. doi: 10.1016/j.ijrmms.2016.11.016

Zheng, C., Yao, Q., Tang, C., Xu, Q., Chong, Z., and Li, X. (2019). Experimental investigation of the mechanical failure behavior of coal specimens with water intrusion. *Front. Earth Sci.* 7:348. doi: 10.3389/feart.2019.00348

Zhou, H., Meng, F., Liu, H., Zhang, C., Lu, J., and Xu, R. (2014). Experimental study on characteristics and mechanism of brittle failure granite. *Chin. J. Rock Mech. Eng.* 33, 1822–1827. doi: 10.13722/j.cnki.jrme.2014.09.012

Zhou, X., Lin, H., and Li, J. (2020). Analysis of internal stress distribution and mechanics characteristics of pre-existing cavity in brittle rock under triaxial cyclic loading. *Front. Earth Sci.* 8:33. doi: 10.3389/feart.2020.00033

Zuo, J., Liu, L., Zhou, H., and Huang, Y. (2013). Deformation failure mechanism and analysis of rock under different mining condition. *J. China Coal Soc.* 38, 1319–1324. doi: 10.13225/j.cnki.jccs.2013.08.013

Conflict of Interest: The authors declare that the research was conducted in the absence of any commercial or financial relationships that could be construed as a potential conflict of interest.